CLM - P 505

CLM - P 505

UKAEA RESEARCH GROUP

Preprint

HEATING AND CONFINEMENT IN THE CLEO STELLARATOR

D W ATKINSON, D BARTLETT,
J BRADLEY, A N DELLIS,
S M HAMBERGER, J B LISTER,
D J LEES, W MILLAR,
L E SHARP, P A SHATFORD.

CULHAM LABORATORY
Abingdon Oxfordshire

1977

HEATING AND CONFINEMENT IN THE CLEO STELLARATOR

D W Atkinson, D Bartlett*, J Bradley, A N Dellis,
S M Hamberger, J B Lister, D J Lees, W Millar,
L E Sharp and P A Shatford.
Culham Laboratory, Abingdon, Oxon, England.
(Euratom/UKAEA Fusion Association)

Invited paper presented to Eighth
European Conference on Controlled Fusion
and Plasma Physics by S M Hamberger.
(To be published in Vol II of Proceedings).

ABSTRACT

The paper presents new results from operation at significantly greater vacuum poloidal fields than were previously available. Plasma density between 0.2 and 6 x 10^{13} cm $^{-3}$, and central electron and ion temperatures up to 900 and 300 eV respectively, can be obtained in pulses lasting up to 0.2 sec. with modest ohmic heating currents (8-20kA) and toroidal fields up to 20 kG. The electron energy replacement time τ_{Ee} is typically 1 - 10 ms, being longest at small ohmic currents. τ_{Ee} generally decreases with increasing drift parameter u/v_e. Soft X-ray and u.v. spectra indicate low impurity content ($Z_{eff} < 1.1$) although the resistance exhibits an anomaly factor typically 2 - 4.

* On leave from Sydney University, Sydney, N.S.W., Australia.

October 1977

HEATING AND CONFINEMENT IN THE CLEO STELLARATOR

D.W. Atkinson, D. Bartlett, J. Bradley, A.N. Dellis, S.M. Hamberger
D.J. Lees, J.B. Lister, W. Millar, L.E. Sharp and P.A. Shatford

Euratom/U K A E A Fusion Association,
Culham Laboratory, Abingdon, Oxon, England

INTRODUCTION

CLEO is a conventional stellarator, having 7-field periods of $\ell = 3$ helical windings wound on a 25 mm thick, stainless steel torus of mean major radius 90 cm and bore 28 cm. When the lobes of the outermost closed magnetic surface (trefoil-shaped) are defined by the 13 cm radius tungsten limiters, the resulting plasma boundary has a mean radius $a \approx 10$ cm.

Recent modifications have for the first time allowed operation at the full helical winding current (120 kAT) with maximum toroidal field $B_\phi = 20$ kG; with the separatrix just inside the limiters the maximum rotational transform due to the vacuum fields is $\iota_0 = 0.6$. The computed magnetic surfaces have been confirmed by experiment using a low velocity electron beam. Most of the results reported here use this field configuration ($I_{eq} \equiv \frac{a^2}{2R} \iota_0 B_\phi \leq 66$ kA), in contrast to that reported earlier[1,2] for which restrictions on the helical winding current limited the transform to $\iota_0 \approx 0.3$ at $B_\phi = 12.7$ kG ($I_{eq} = 21$ kA).

Many of the trends reported here, e.g. the improvement in confinement at low currents, were suggested in the earlier results but the limited operating range did not allow them to be positively confirmed.

Ohmic heating currents lasting up to 0.2 s are obtained using a series of up to 6 electrolytic capacitor banks discharged into a 12-turn primary winding on a two-limbed iron transformer core (0.8 Vs).

The principal diagnostics include: a single-channel 2 mm microwave interferometer producing a direct reading display of mean density; photon scattering (5 J ruby laser) for profiles of T_e and n_e, measured at

$R = 90$ cm along a vertical radius above the horizontal median plane; soft X-ray emission from minor radii between $r = \pm 7$ cm (vertically) using uncooled Si detectors and foil absorbers; energy spectra of neutral particles emitted both radially and tangentially; horizontally viewed electromagnetic emission spectra from 30 to 300 GHz (cyclotron radiation) using Fourier transform spectroscopy; absolute H_α emission from plasma regions both close to and remote from a limiter; quartz and grazing-incidence vacuum ultra-violet line emission; and a sensitive multi-channel 2 mm interferometer used to study density fluctuations in the outer plasma regions.

OPERATION WITH OHMIC DISCHARGES

'Clean' vacuum conditions are obtained by continuous titanium gettering over about half the internal surface of the torus between discharges, rapid discharge cleaning being necessary only following initial pump-down The normal operating base pressure is $\sim 5 \times 10^{-8}$ torr, the residual gas consisting mainly of water vapour.

Operation at the significantly larger poloidal fields than were previously available[1,2] allows the ready production of well-behaved, long duration discharges whose boundary is close to the computed separatrix. This contrasts with the operation at lower I_{eq} when it was found necessary to apply a programmed vertical field proportional to the current I_g in order to obtain equilibria. This is now attributed to the effect of a leakage field from the transformer on the magnetic surfaces, whose effect becomes weak at low I_g and high I_{eq}.

Hydrogen gas is admitted from three pre-programmed electromechanical valves. Breakdown occurs readily for initial pulsed fillings of $\sim 10^{-4}$ torr H_2 and low loop voltages ($V \leqslant 15$ V) with little evidence of runaway production, as inferred from the absence of hard X-ray and non-thermal e.m. emission. The low wall recycling rate resulting from the gettered surface allows the subsequent density to be controlled by a carefully distributed gas influx. The maximum rate of density increase depends on the gas current, too great a neutral influx quenching the discharge. For typical pulse lengths $\sim 150 - 200$ ms maximum mean densities achieved in this way range from $\bar{n}_e \sim 3 \times 10^{13}\,\mathrm{cm}^{-3}$ at $I_g = 10$ kA to $\sim 6 \times 10^{13}\,\mathrm{cm}^{-3}$ at 25 kA, while much lower, steady densities, e.g. $\bar{n}_e \sim 5 \times 10^{12}\,\mathrm{cm}^{-3}$, can be made reproducibly and free of runaways.

Some typical oscillograms illustrating two operating conditions are shown in Fig.1(a) and (b), Fig.1(b) showing the effect of too great a gas influx which quenches the discharge.

The results quoted here have all been obtained with the vacuum magnetic fields chosen so as to place the separatrix just inside the limiter; under these conditions the H_α emission is not enhanced at the limiter, indicating the detachment of the plasma from the material wall (i.e. the plasma is defined by a magnetic limiter). This implies that the ionization is essentially uniform azimuthally and thus allows a reasonable estimate of the total hydrogen ionization rate, and thus the particle confinement time τ_p, to be obtained.

Electron density and temperature profiles (Fig.2) are obtained by optically imaging different parts of the ruby laser beam which traverses a vertical diameter at $R = 90$ cm on to the entrance slit of the receiving spectrograph; this allows measurements between the horizontal axis and the upper plasma boundary with a spatial resolution of ~ 1 cm. The density distribution is always fairly flat, and similar to those found earlier with the separatrix outside the limiter, while the temperature profile is narrower.

Under some conditions, difficulty has been found in fitting the observed scattered spectra to simple Maxwellian distributions, a significantly higher temperature 'tail' being apparent – this effect is not seen near the centre of the plasma ($r = 0$) but is quite pronounced at radii $\sim 2 - 4$ cm. Since we have not yet resolved whether this is due to a genuine non-Maxwellian electron distribution or due to instrumental error, we show in Fig.2(a) two limiting profiles which are consequences, (i) of fitting the best Maxwellian to the data, representing an *upper* limit on the true temperature; (ii) of neglecting the signals in the outer channels (i.e. those associated with the higher energy electrons) and so finding a *lower* temperature limit. The resulting profiles are shown in Fig. 2(a). In what follows we shall, for the sake of caution, assume that the temperature profile has the narrower shape (ii), so that, e.g., energy confinement times based on this profile may well be an underestimate.

Notice that the temperature profile can be measured with the laser only along a vertical chord at $R = 90$ cm, while the maximum current density,

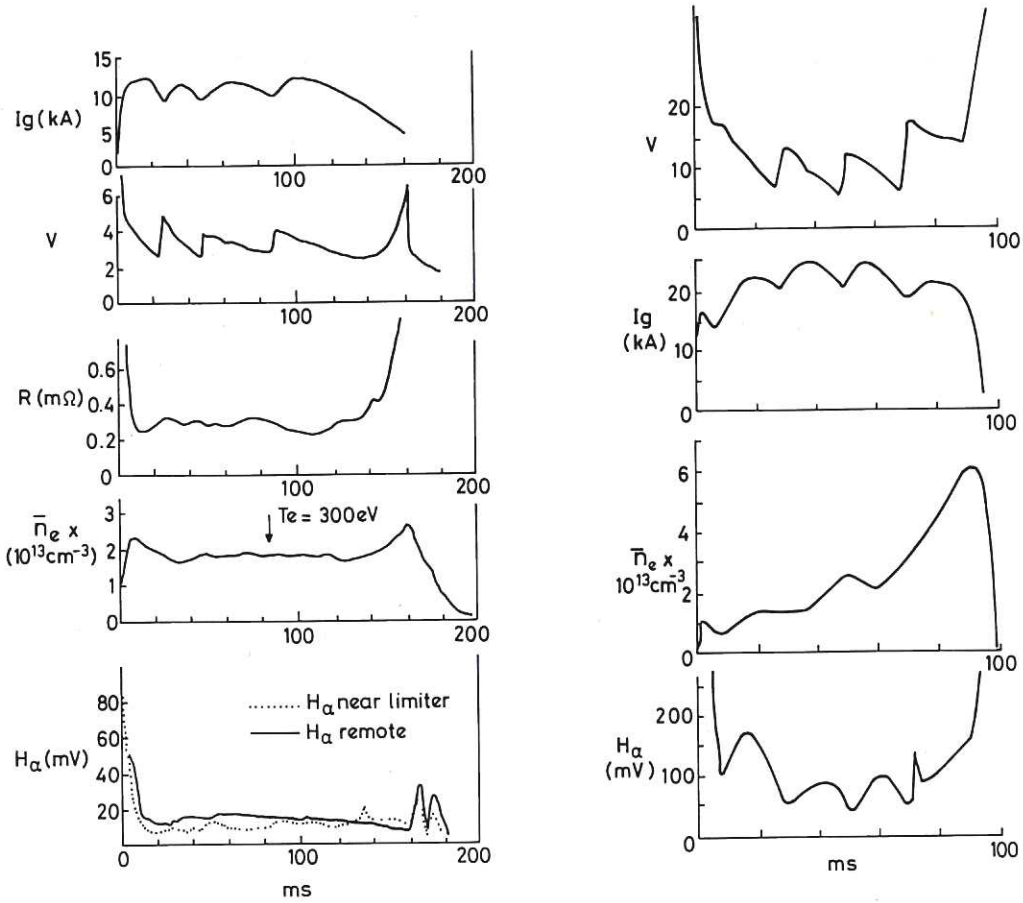

Fig.1
Oscillograms under two typical conditions
(a) Shot 4599. B_ϕ = 18 kG, τ_0 = 0.6, one gas valve only.
(b) Shot 3389. B_ϕ = 16 kG, τ_0 = 0.6, with auxiliary gas puffing 30 ms after discharge initiation.

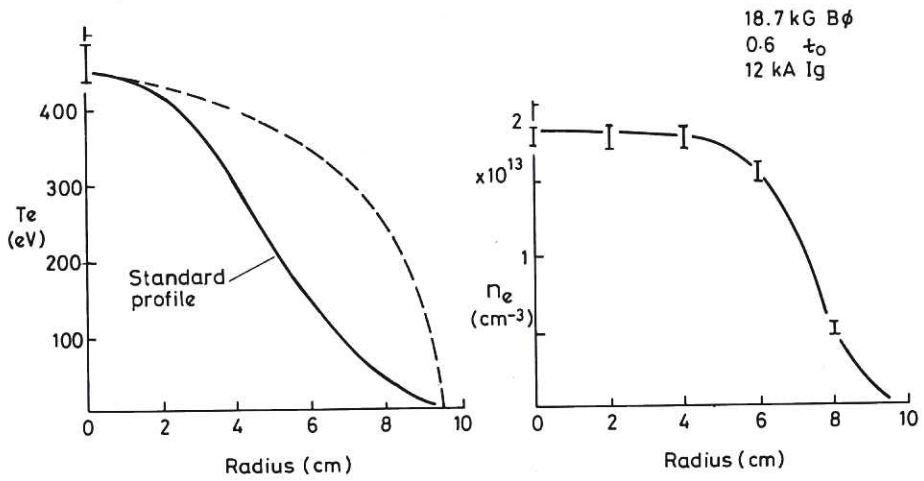

Fig.2
Radial profile of (a) electron temperature
(b) electron density; B_ϕ = 18.7 kG, I_g = 12 kA
and τ_0 = 0.6.

CLM-P505

(corresponding to the self-consistent magnetic axis) could occur at $R > 90$ cm, so that the laser measurement may well underestimate the peak temperature when the profile is not flat.

The approximate effect of the azimuthal current on the total rotational transform is shown in Fig.3 for $B_\phi = 18.7$ kG and current direction such as to add to the transform; the contribution due to the current is based on type (ii) temperature profiles together with the usual assumptions on current distribution.

HEATING AND CONFINEMENT

Confinement times have been derived in the following way for the parameter ranges given in Table I.

τ_{Ee} is the simple electron energy replacement time defined by

$$\frac{d}{dt}(W_e) + \frac{W_e}{\tau_{Ee}} = I_g\left(V - I_g \frac{dI_g}{dt}\right)$$

where

$$W_e = 3\pi^2 R_0 \int_0^a r\, n(r)\, T_e(r)\, dr = A \bar{n}_e \hat{T}_e$$

is the total electron energy, $n(r)$ and $T(r)$ have the forms given by Fig.2, $\bar{n}_e$ and $\hat{T}_e$ are respectively the mean electron density (from interferometry) and central temperature (laser), A then being a shape factor taken as constant. In general the time dependent terms in the above relation were very small. Notice that, as defined, τ_{Ee} excludes ion energy and includes inelastic collisions and radiative power losses in the power input term.

TABLE I

Parameter	Range
Mean density $\bar{n}_e$ (cm^{-3})	$3 \times 10^{12} - 6 \times 10^{13}$
Central electron temperature T_e (eV)	100 - 1000
Ion temperature T_i (eV)	80 - 300
Toroidal field B_ϕ (kG)	14 - 20
Vacuum transform at separatrix ι_0	0.6
Plasma current I_g (kA)	8 - 25
*Collisionality $\frac{\nu}{\nu^*} = \frac{R}{\bar{\iota}\,\bar{\lambda}_{mfp}}$ (electrons)	$10^{-4} - 3 \times 10^{-1}$
Collisionality " " (ions)	$10^{-3} - 10^{-1}$
Electron drift/thermal velocity $\overline{v_d/v_e}$	0.01 - 0.3
Equivalent current I_{eq}	46 - 66

*Averaged over $|r| \leq 5$ cm, assuming $Z = 1$

Generally it is found that both energy and particle confinement improve as the current decreases and as the density increases. As a result of this, roughly similar temperature and density can be obtained for a wide range of ohmic heating current (in contrast to the usual situation in a tokamak where the heating and confining currents cannot be separated). This trend is illustrated in Fig.4, which shows the electron energy replacement time τ_{Ee} for various currents for two sets of plasma conditions. At the largest currents used τ_{Ee} approaches values typical of stellarators with $I_g \sim I_{eq}$, i.e. about those for the equivalent tokamak[2,3]. The range of values corresponding to the empirical tokamak scaling law of Hugill and Sheffield[4] for the total energy confinement time

$$\tau_E(\text{ms}) = 2.7\ n_{13}^{0.61}\ a^{1.57}\ B_3^{0.88}$$

($n_{13} = n_e \times 10^{-13}$, a = radius in m, $B_3 = B_\phi$ in kG) are shown for comparison. However, at the lowest currents used, where the vacuum fields dominate the transform, the energy confinement increases to significantly higher values.

The effect on τ_{Ee} of increasing the magnetic field strength for low current discharges at roughly similar density and temperature, is shown in Fig.5. This strong dependence (approximately $\tau \propto B_\phi^2$), is not, however, found when larger currents ($\geqslant 20$ kA) are used (dashed error bars).

The overall effect of different densities, current and temperature conditions can be seen by plotting τ_{Ee} against the drift parameter $\xi \equiv v_d/v_e \propto I/n\,T_e^{\frac{1}{2}}$. This is shown in Fig.6, which uses data from ~ 150 discharges with the same t_0, but with other parameters as in Table I. This plot, which is qualitatively like that found in TORSO[1,5] indicates a clear trend towards poorer confinement at large drift parameters.

Particle confinement times, obtained using hydrogen ionization rates derived from the H_α emission and neglecting any contribution from impurities, are shown plotted in the same way in Fig.7. These exhibit essentially the same trend, but with absolute values considerably longer than τ_{Ee}.

Ion temperatures, derived in the usual way from the neutral particle analyzers, vary between 80 and 300 eV. For most operating conditions the measured values are within a factor of two of estimates based on the usual Artsimovich scaling law, but at lower densities there is some indication of enhanced ion-heating, (Fig.8).

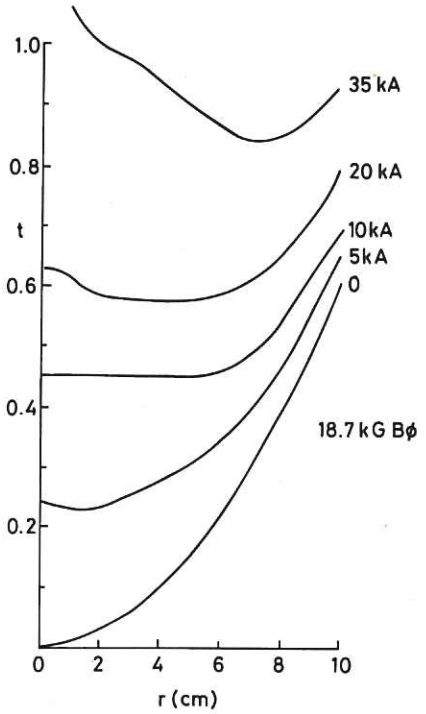

Fig.3
Radial dependence of rotational transform for B_ϕ = 18.7 kG and different values of plasma current, based on standard profile of Fig.2(a).

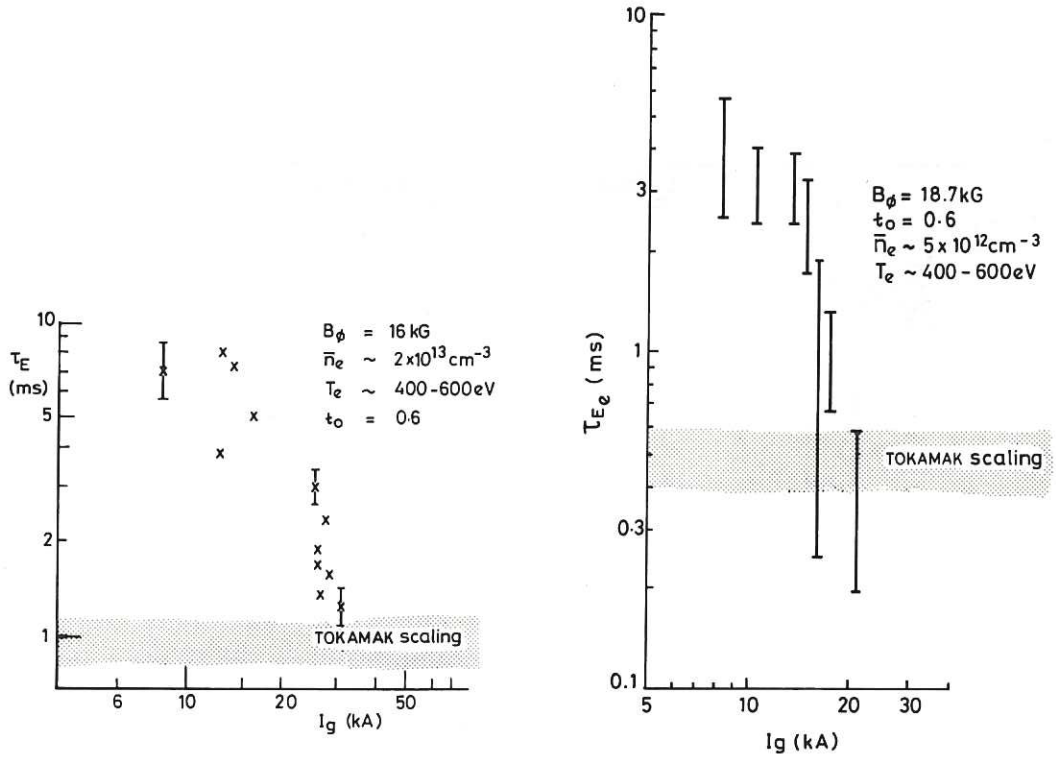

Fig.4
Variation of energy replacement time τ_{Ee} with plasma current for two different conditions of density and temperature.

CLM-P505

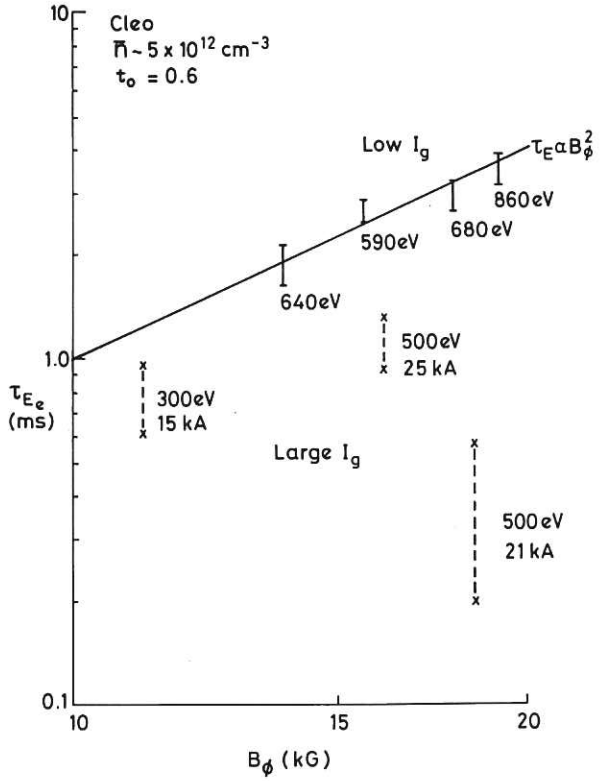

Fig.5
Variation of electron energy replacement time with toroidal field.

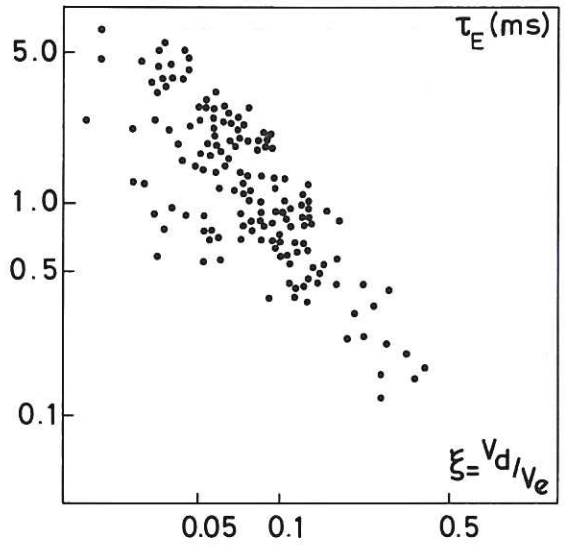

Fig.6
Variation of electron energy replacement time with mean drift parameter $\overline{v_d/v_e}$.

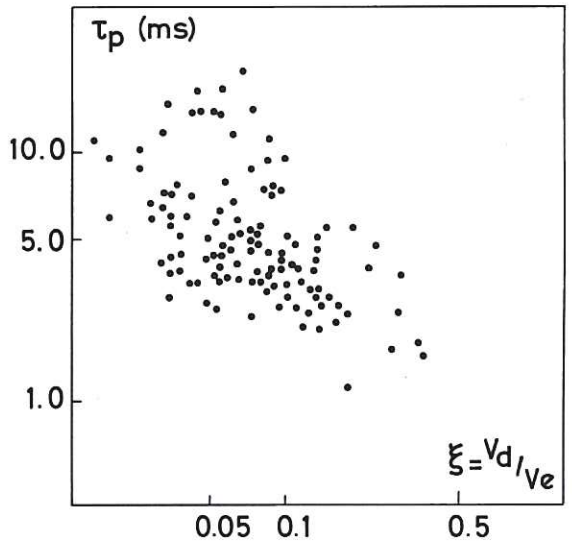

Fig.7
Variation of particle containment time with mean drift parameter $\overline{v_d/v_e}$.

CLM-P505

A comparison with the pseudo-classical scaling law, which should result in the proportionality

$$W \propto I_g(I + I_{eq})$$

is shown in Fig.9, where the earlier data has been indicated by different symbols. This plot suggests that the apparent pseudo-classical dependence found in the early data was fortuitous, and resulted from the experimentally unavoidable inter-dependence of density and current which no longer applies under present conditions.

Some representative plasma conditions are shown in Table II.

TABLE II

Shot Number		3514	4400
B_ϕ	(kG)	15.7	18
τ_0		0.6	0.6
$\bar{n}_e$	(10^{13} cm^{-3})	1.8	0.5
$\hat{T}_e$	(eV)	540 ± 40	620 ± 80
T_i	(eV)	170	120
V_R	(V)	2.4	2.8
I_g	(kA)	12.0	10.5
τ_{Ee}	(ms)	9.5 ± 1.1	3.2 ± 0.5
Z_R		3.2	4.0
τ_p	(ms)	~ 34	~30
$\beta_{\phi e}$		1.6 ± 10^{-3}	4×10^{-4}
τ_{Ee}/τ_{Bohm}		~100	~40

PLASMA PURITY AND RESISTANCE

Absolute measurements of the soft X-ray emission spectra, made by pulse height analysis using the cooled detector, are shown in Fig.10 for a typical discharge condition. The emission is only slightly above that expected for pure hydrogen bremsstrahlung with the profiles used, the X-ray anomaly factor being $A_x = 4.3$ corresponding to $Z_{eff} \leqslant 1.05$ (assuming the increase is due to oxygen recombination radiation). The value of electron temperature derived from the slope is somewhat higher than that measured by the laser at $R = 90$ cm, consistent with a horizontal displacement of the central (hottest) region.

The above result also agrees with an estimate of the oxygen impurity concentration based on the absolute emission of the OVIII resonance line at 23 Å, viz $N_{oxygen} \not> 2 \times 10^{10}\,cm^{-3}$, so that $Z_{eff} \leqslant 1.1$. Photographic records of grazing incidence emission lines show a very low level of metal impurity.

The measured plasma resistance, however, generally shows a resistive anomaly Z_R between 2 and 4 times larger than that calculated for pure hydrogenic plasma ($Z = 1$) with local conductivity given by the Spitzer value based on the measured central electron temperature and the assumed profile, but taking no account of e.g. trapped particle effects. The greatest resistive anomaly occurs at low currents and high temperatures; unfortunately the T_e profiles are not sufficiently accurately known to determine whether this anomaly is real.

ELECTRON CYCLOTRON EMISSION

Electromagnetic emission spectra encompassing the first three harmonics of the electron cyclotron frequency are obtained, with 14 ms time resolution, using the mechanically scanned interferometer system described elsewhere[6]. A typical spectrum is shown in Fig.11, and is consistent with a thermal electron distribution without enhancement due to collective effects. The peak electron temperature derived from the second harmonic component of the emission is always proportional (within ± 25%) to the central temperature measured by the laser; however, using the precise resonance condition $\omega = 2\omega_{ce}$ to find the position corresponding to this peak, shows it to occur some 2 - 3 cm outwards from the geometric axis, i.e. at R = 92 - 93 cm. Even at densities as low as $n_e \approx 5 \times 10^{12}\,cm^{-3}$, provided low loop voltages ($V \leqslant 15$ eV) are used, non-thermal effects due to runaways disappear in less than 50 ms after the discharge is initiated. When steady conditions are maintained throughout the pulse the emission remains constant, showing that the electron temperature, within the 14 ms time resolution available, remains the same.

Temperature profiles derived on the usual assumption that the plasma everywhere radiates as a black body are shown in Fig.12, with appropriate laser temperature data (normalized) for comparison. However, at the low densities for which this diagnostic has so far been employed ($n < 2 \times 10^{13}$ cm^{-3}) the plasma is insufficiently locally absorbing, except perhaps at

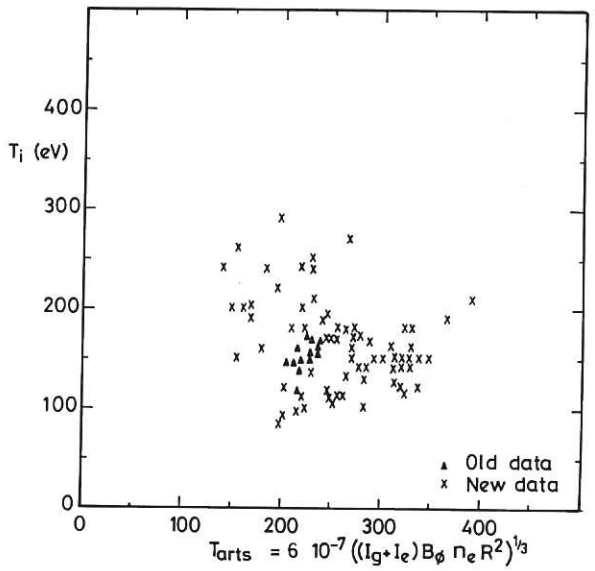

Fig.8
Ion temperature T_i versus the Artsimovich scaling parameter. The full line is drawn through the previous experimental data[1,2] and lies a factor of two below the true Artsimovich scaling.

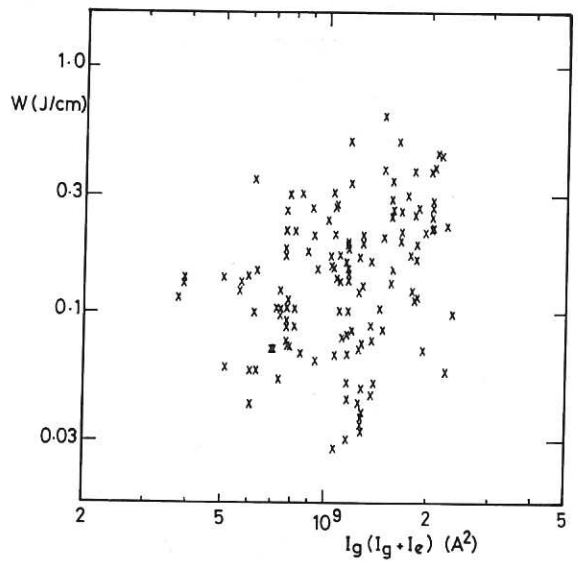

Fig.9
Electron energy per unit length W_e versus the pseudo-classical scaling parameter. I_E is the equivalent current due to the vacuum transform

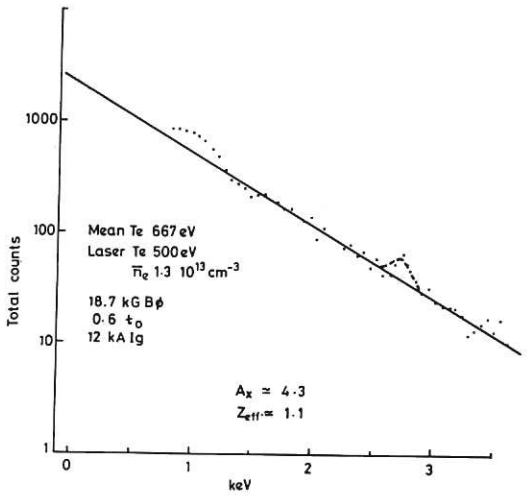

Fig.10
Spectrum of soft X-radiation as measured by Si(Li) cooled detector.

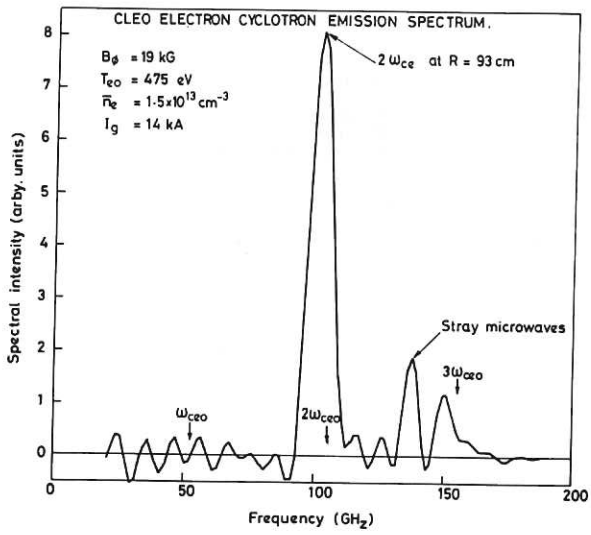

Fig.11
Typical electron cyclotron emission spectrum for the conditions B_ϕ = 19 kG, T_e = 475 eV (by photon scattering), $\bar{n}_e$ = 1.5×10^{13} cm^{-3}.

CLM-P505

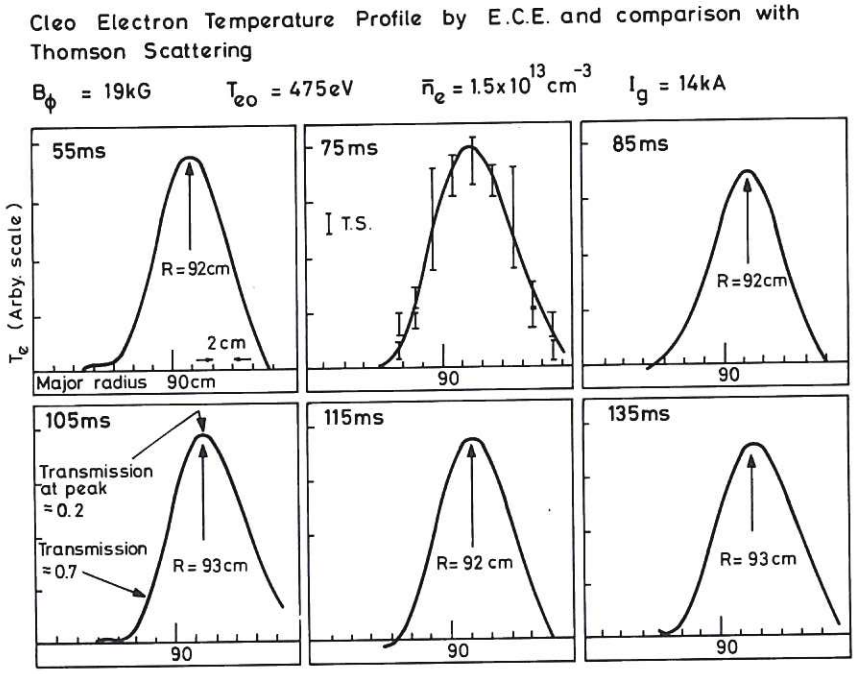

Fig.12
Time resolved radial profiles of electron temperature derived from electron cyclotron emission. A comparison is made between the profile at 75 ms and the data used for Fig.3(a).

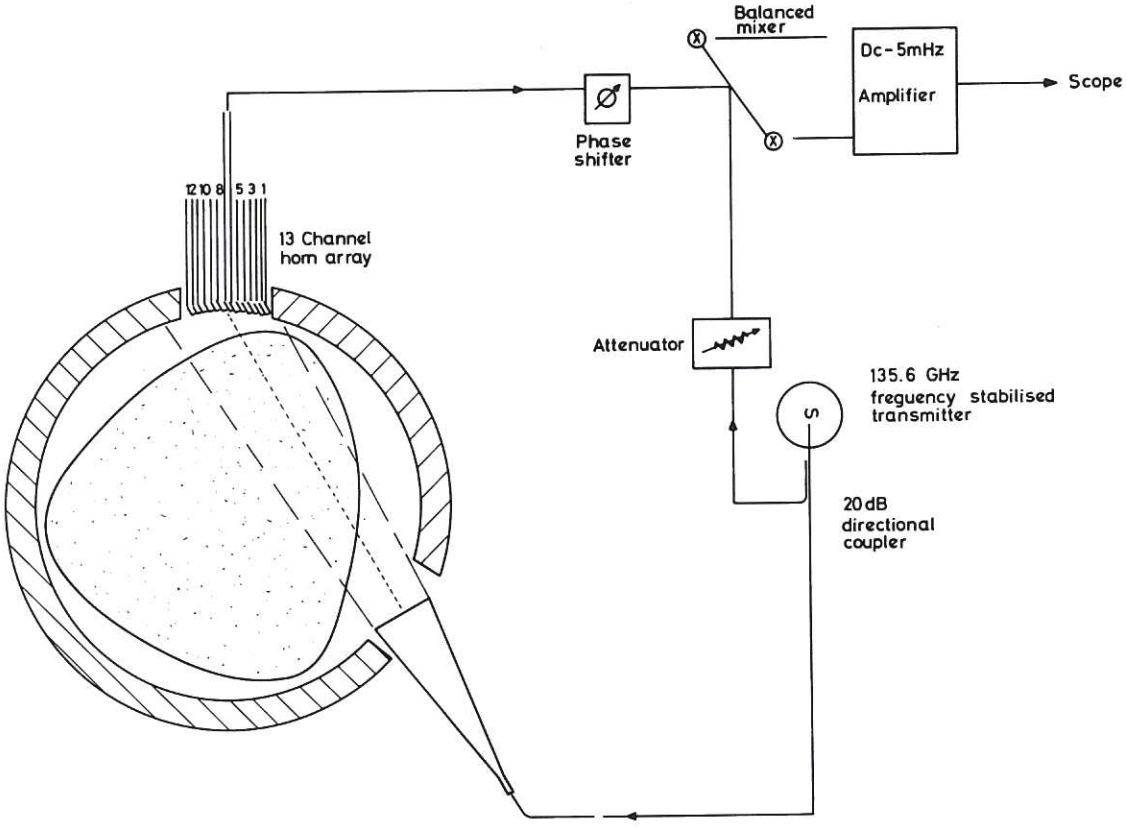

Fig.13
Schematic arrangement of the apparatus for measuring density fluctuations.

CLM-P505

the centre, for this apparent agreement to be relied on, since the low opacity in the outer regions can lead to an under-estimate of the profile width.

DENSITY FLUCTUATIONS

The arrangement shown schematically in Fig.13 has been installed to observe density fluctuations in the outer region of the plasma in an attempt to examine these as a possible cause of the enhanced diffusion at higher plasma currents. A 2 mm microwave beam about 7 cm wide traverses the plasma, entering as an essentially plane wave and emerging with phase variations across the beam caused by the fluctuations. The phase is recorded with time resolution $\sim 10^{-6}$ s at up to 8 positions across the beam by a set of 13 receiving antennae, wavelength and frequency spectra of the fluctuations being related to appropriate time and position correlations of the received signals.

A preliminary example of recorded signal is shown in Fig.14 for seven such channels. There appears to be more than one type of fluctuation present simultaneously, e.g. the signals show coherent, harmonic oscillations at $\sim$20 kHz, well correlated for transverse distances > 3 cm, and with amplitudes $\delta n/n \sim 3\%$ which disappear when the current decays in the afterglow, while at the same time incoherent oscillations, with much smaller scale length and broad frequency spectra (up to 120 kHz) can be observed. Magnetic probes outside the plasma show that the 20 kHz density oscillations are well correlated with fluctuations in the poloidal field, with $\delta B_\theta/B_\theta \sim 1\%$.

DISCUSSION AND CONCLUSIONS

Although there inevitably remains some residual uncertainty about the absolute values of the electron energy replacement time resulting from uncertainty in interpreting the laser scattering data, the general trends are clear, namely:

1. That the energy confinement is improved when operating at low ohmic heating currents, i.e. with the vacuum magnetic fields essentially determining the particle confinement in the outer regions.
2. The confinement at a given (low) current improves significantly with the magnetic field strength, when the plasma density and temperature are held approximately constant.

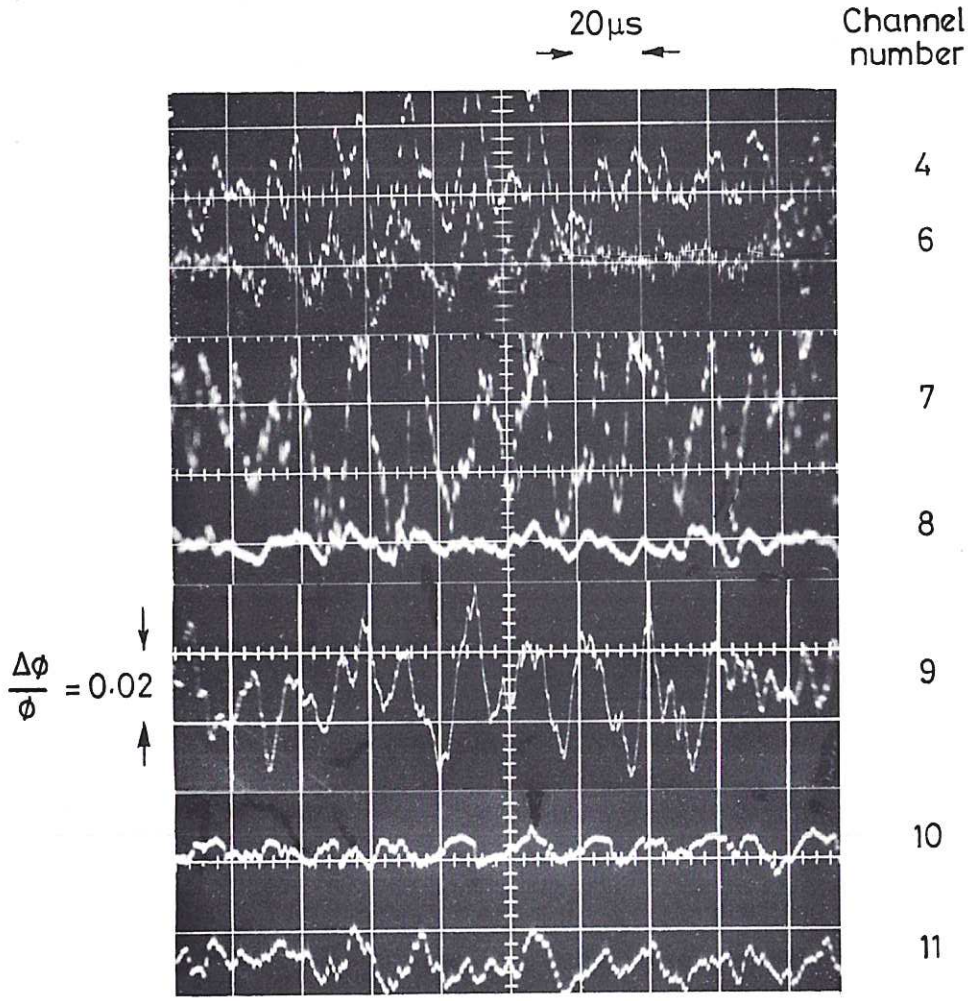

Fig.14
Oscillograms of raw data produced by the arrangement in Fig.13. The phase changes are shown for 7 separate channels. Abscissa 20 μs/div.

CLM-P505

3. The confinement is noticeably worse when the drift parameter v_d/v_e, is larger, although no physical explanation is as yet available to justify this dependence.

4. There is a variety of fluctuations present in the outer density region, whose relation (if any) to the confinement has yet to be explored.

5. The plasma, presumably as a result of the surface gettering, appears to be almost free of impurity. However, under some conditions of current and temperature the measured plasma resistance is higher than expected. Further work is needed to ascertain whether there is a genuine resistive anomaly or whether this reflects a constriction of the current narrower than can be explained by the temperature profile data presently available.

6. Because the temperature gradients are not yet sufficiently well known to derive experimental heat conductivities it is not meaningful to make proper comparison with neo-classical transport theory.

7. Operation over a much wider range of parameters than was previously possible shows that the confinement is no longer consistent with the semi-empirical pseudo-classical scaling law found at high current operation and a very restricted parameter range[1] (see Fig.9).

ACKNOWLEDGEMENTS

The team wish to thank R.J. Bickerton for his constant encouragement, K. Axon and R.D. Gill for the soft X-ray spectrum and its interpretation, and A. Costley and the National Physical Laboratory, Teddington, England, for the loan of the scanning microwave interferometer.

REFERENCES

(1) ATKINSON, D.W. et al. Plasma Physics and Controlled Nuclear Fusion Research, 1976, vol.II.

(2) ATKINSON, D.W. et al., Phys. Rev. Lett., 37, 1616 (1976).

(3) BLAUMOSER et al., WVII A Team, Plasma Physics and Controlled Nuclear Fusion Research, 1976, IAEA, vol.II, p.81.

(4) HUGILL, J. and SHEFFIELD, J., Nuclear Fusion (to be published)

(5) HAMBERGER, S.M. et al., Phys. Rev. Lett., 37, 1345 (1976).

(6) COSTLEY, A.E. and TFR Group, Phys. Rev. Lett., 38, 1477 (1977).